Is Excited State Aromaticity a Driving Force for Planarization of Dibenzannelated 8π-Electron Heterocycles?

Josene Toldo,[1] Ouissam El Bakouri,[1] Miquel Solà,[2] Per-Ola Norrby,[3] and Henrik Ottosson[1]*

[1] Department of Chemistry - Ångström Laboratory, Uppsala University, Box 530, 751 20 Uppsala, Sweden, [2] Institute of Computational Chemistry and Catalysis and Department of Chemistry, University of Girona, C/ M. Aurèlia Capmany, 69, Girona, 17003, Spain, [3] Early Product Development, Pharmaceutical Sciences, IMED Biotech Unit, AstraZeneca, Gothenburg, Sweden

Abstract: Compounds with dibenzannelated heterocycles with eight π-electrons are found in a range of applications. It was argued by Shukla and Wan [*J. Am. Chem. Soc.* **1993**, *115*, 2990] that two such compounds, dibenz[*b,f*]oxepine and dibenz[*b,f*]thiepin, adopt planar structures in their lowest singlet excited states due to "attainment of a cyclically conjugated system of 8π electrons in the central ring". Herein we report on a quantum chemical investigation of the aromatic character in the first excited singlet and triplet states (S_1 and T_1) of dibenzannelated seven- and six-membered heterocycles with one, two or three heteroatoms in the 8π-electron ring. The S_1 and T_1 states could have ππ* or nπ* character, and we find that compounds with one or two heteroatoms in the central ring have ππ* states as their S_1 and T_1 states. These states are to a significant degree influenced by excited state aromaticity, and their optimal structures are planar or nearly planar. Among the heteroatoms, nitrogen provides for the strongest excited state aromaticity whereas oxygen provides for the weakest, following the established trend of

the electronic ground state. Yet, dibenzannelated seven-membered ring compounds with N=N bonds have nonaromatic nπ* states with strongly puckered structures as their S_1 and T_1 states.

Introduction

A change in aromaticity is one of the most powerful driving forces to control and modulate reactivity, structure and other molecular properties.[1] In the ground state (S_0), Hückel's rule tells that aromaticity is associated with fully conjugated cycles with $4n + 2$ π-electrons,[2] and it has had a profound impact on our understanding of various chemical reactions and molecular properties. A change in aromaticity in the lowest electronically excited states, as given by Baird's 4*n* rule,[3,4] can similarly be a driving force for photoreactivity and changes in excited state properties.[5,6] Baird's rule was formulated for the lowest ππ* triplet state (T_1), yet, it has been found through computations that it often extends to the lowest singlet excited state (S_1) of small annulenes.[7,8] Thus, annulenes with $4n$ π-electrons can be aromatic in their T_1 and S_1 states.

The focus herein is on the excited state aromaticity of dibenzannelated molecules with central 8π-electron rings. Compounds of this type are found in a wide range of applications, for example in antipsychotic drugs such as quetiapine and chlorpromazine (Figure 1), and in photofunctional molecular materials for usage as viscosity probes and photoresponsive liquid crystals.[9,10] Dibenzo[*b*,*f*][1,4]oxazepin is a very strong lachrymatory agent known as CR gas, and dibenzodioxin is the core in some of the most environmentally hazardous polychlorinated chemicals known. Finally, oxepin units situated at the edges of graphene nanosheets as cyclic ethers, effectively benzannelated oxepins, have been proposed as the cause for exciton self-trapping observed in graphene quantum dots and carbon dots.[11]

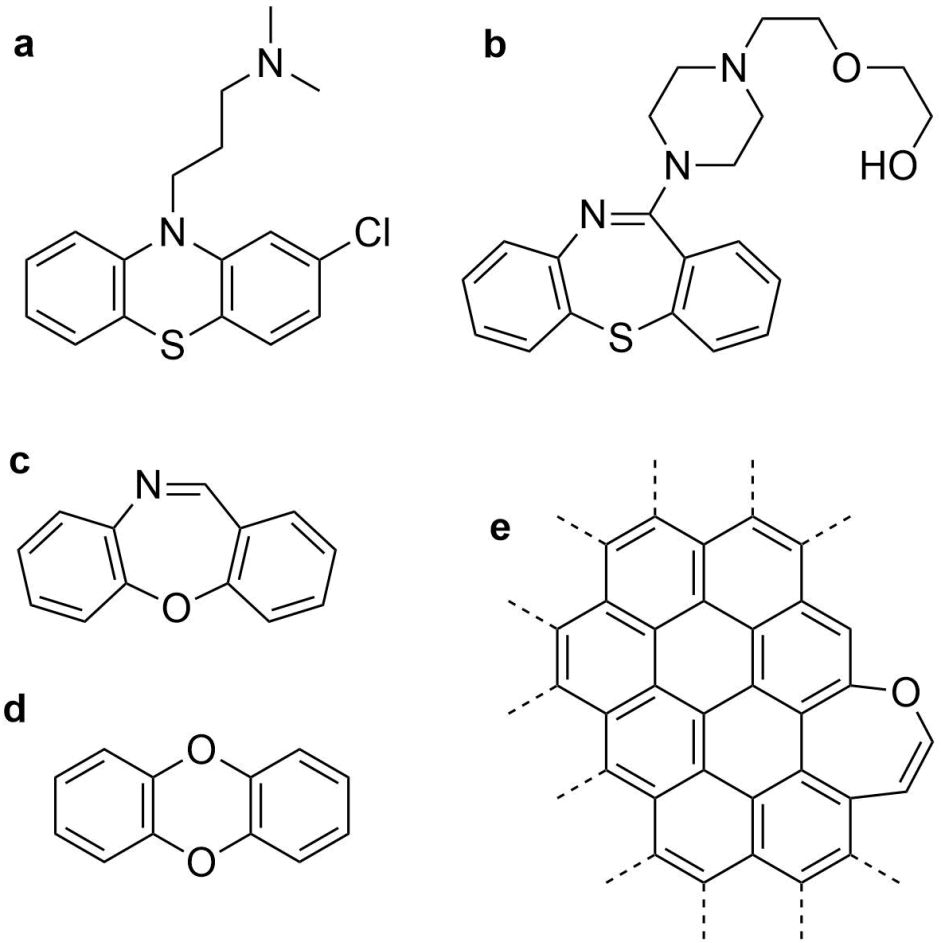

Figure 1: Molecules containing central 8π-electron rings: (a) chlorpromazine, (b) quetiapine, (c) dibenz[*b,f*][1,4]oxazepine (CR gas), (d) dibenzodioxin, and (e) an edge-oxidized graphene nanosheet.

Cyclic 8π-electron molecules in their S_0 states normally adopt non-planar structures that are non-aromatic rather than antiaromatic. Cyclooctatetraene (COT) in S_0 adopts a tub-shaped geometry, avoiding the angle strain at the planar D_{4h} symmetric structure,[12] and also azepines, oxepines, and thiepines adopt puckered conformations.[13-19] The resonance energies of the planar structures of azepine and oxepines obtained through extended Hückel MO theory and early Hartree-Fock computations suggested antiaromatic character, [20,21] later supported by NICS calculations.[14,22] However, the dibenz[*b,f*]annelated derivatives were found to have positive resonance energies associated with some aromatic character as their benzene rings

keep their Hückel aromaticity in line with Glidewell-Lloyd's extension of Clar's rule.[23,24] Still, dibenzo[*b,f*]oxepin, similarly to oxepin, adopts a saddle-shaped structure in the S_0 state.[4] Also dibenzannelated 8π-electron six-membered ring compounds such as phenothiazine and phenoxepine adopt nonplanar conformations in S_0.[25]

Yet, Baird's rule can lead to aromatic stabilization and planarization of many of these molecules in their lowest excited states. Quantum chemical calculations tell that COT in the S_1 and T_1 states exhibits planar D_{8h} structures and magnetic properties typical of high degree of aromaticity.[7,8,26-28] Several experimental observations related to large structural changes in the excited states, when compared to the S_0 state, have been reported for COT and a number of COT derivatives.[9,29,30] With regard to dibenzannelated heterocycles, dibenz[*b,f*]oxepin displays a large Stokes' shift and well-defined vibrational fine structure in the fluorescence spectrum, evidences that a change from a V-shaped to a planar conformation occurs in the S_1 state (Figure 2),[31] and similar findings were made for dibenz[*b,f*]thiepin. Interestingly, dibenz[*b,f*]oxepin shows an increased photostability when compared to its 10,11-dihydrogenated analogue,[31] a feature that could be connected to the gain in S_1 state aromaticity of a cyclic system with 4*n* π-electrons. More recently, it was possible to obtain an experimental assessment of excited state aromatic stabilization in a chiral COT derivative.[29] The racemization enthalpy determined through time-resolved CD spectroscopy of the isolated enantiomer revealed its excited state aromatic stabilization to be 21 – 22 kcal/mol in both the T_1 and S_1 states.

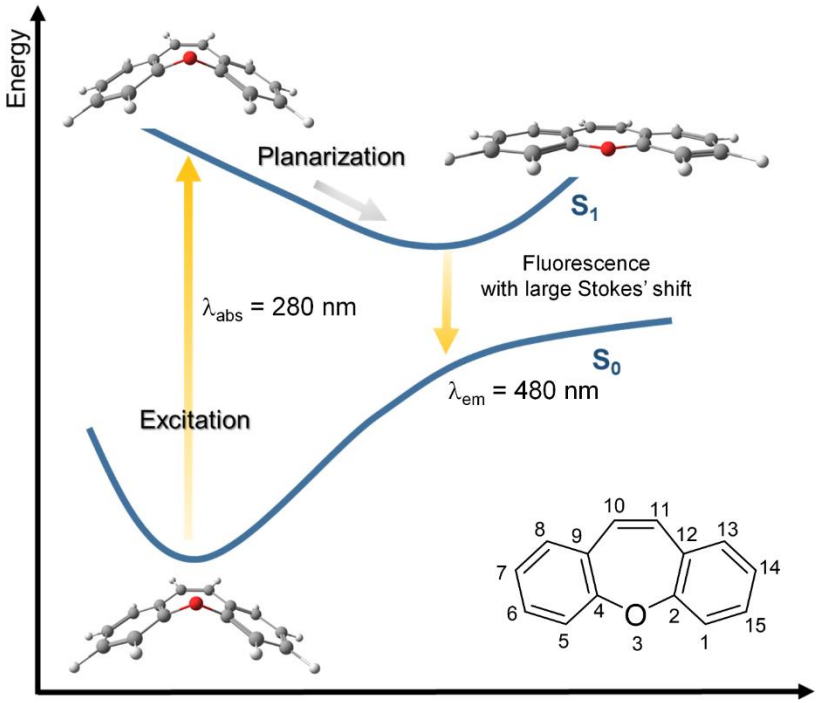

Figure 2. Schematic representation of the potential energy surfaces for planarization of dibenzo[*b,f*]oxepin in the S_1 state and the absorption and emission wavelength from ref. 31.

Yet, there are also limitations to the excited state aromaticity concept. The presence of an 8π cyclooctatetraene ring in the center of acene dimers is not a guarantee for planarization in the S_1 state, as it depends on the acene length.[6] Also, is there a similarity in the degree of aromaticity between azepines, oxepines and thiepines in the T_1 and S_1 states as there is between pyrrole, furan, and thiophene in the S_0 state? Finally, with more C atoms exchanged to heteroatoms there will be an increase in the number of nπ* states, and they may become the S_1 and T_1 states. Herein we report on a computational study in which we probe if gain of excited state aromaticity, as given by Baird's rule, is a general driver for planarization in the lowest excited states of dibenzannelated 8π-electron heterocycles. The compounds can tentatively be described as aromatic chameleon compounds (Figure 4),[32,33] that is, compounds that can adapt their electronic structures so as to comply with the different aromaticity rules in different

electronic states: Hückel's rule in S_0 with two π-sextets and Baird's rule in T_1 and S_1 with a π-octet, π-duodectet or π-hexadectet. Besides providing information on the scope and limitations of the excited state aromaticity concept to tricyclic molecules with overall 16 π-electrons, the study also provides insights of the structure-property relationship of molecules that can be of interest in the design of new drugs and photoactived materials. Molecules with aromatic S_1 and T_1 states may display higher photostability than molecules with nπ* states as their lowest excited states.[31] Such findings could be of relevance for targeted design of compounds with improved photostability, or the opposite, increased photoreactivity.

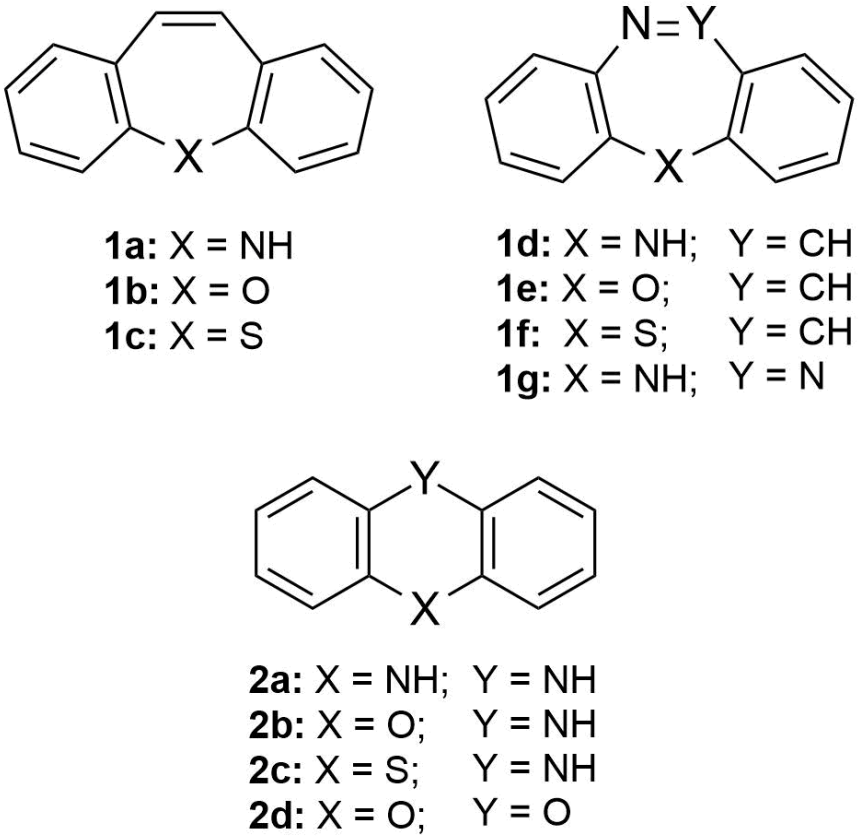

Figure 3. Molecules investigated in this work.

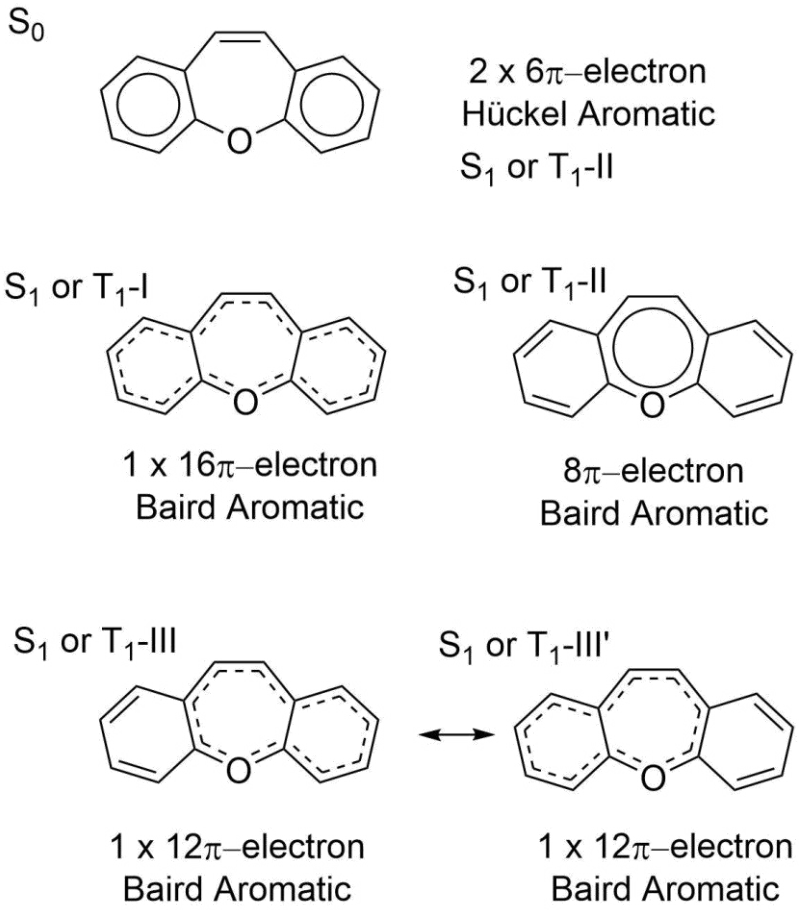

Figure 4: Aromatic resonance structures of dibenzo[*b*,*f*]oxepin in the S_0, S_1, and T_1 states showing that it can act as an "aromatic chameleon" compound.

Computational Methods

Geometry optimizations for the S_0, S_1, and T_1 states were carried out using the PBE0[34] functional and the 6-311+G(d,p)[35] basis set. For selected structures, the effect of dispersion corrections was analyzed by including the GD3 version of Grimme's dispersion model.[36] However, no significant changes were observed in the geometries of S_0, S_1, or T_1 (see Figures S6 to S10 in the Supporting Information). Time-dependent DFT (TD-DFT) was used for the S_1 state optimizations while the unrestricted version of DFT was used for T_1 state optimizations. The PBE0 functional was chosen based on benchmark papers for heterocyclic rings.[37-39] Stationary points with no imaginary frequencies were confirmed through frequency

calculations. The stability of the wave function and spin contamination for the triplet state were checked. Vertical absorption and emission energies were computed at ωB97XD/6-311+G(d,p)//PBE0/6-311+G(d,p) level, having a good agreement with experimental results[40] (see Table S2 in the Supporting Information). CASSCF/6-31G(d) including all the π-orbitals in the active space were carried out at TD-PBE0 geometries to evaluate the configurational weights and verify the character of the S_1 state. For molecules containing seven and six members in the central ring the active space used was 16 electrons in 15 orbitals (CASSCF(16,15) and 16 electrons in 14 orbitals (CASSCF(16,14), respectively. For all the molecules investigated, the S_1 state has a single-configurational character, and with regard to the triplet states all molecules with ππ* T_1 states have $<S^2>$ below 2.0014. CASSCF energies were corrected using CASPT2/6-31G(d) (using an imaginary shift of 0.1 and a standard IPEA value of 0.25). The CASSCF wave function was also used for computing MCI indices at the S_1 state of a few molecules (see below).[41] For all the compounds, TD-DFT emission energies are in good agreement with CASPT2 emission energies and a comparison of the molecular orbitals and states show that TD-DFT is appropriate for the molecules studied. All DFT and TD-DFT calculations were performed with Gaussian 16 revision B.01[42] while OpenMolcas version 18.09 was used for CASSCF and CASPT2 calculations.[43]

The harmonic oscillator model of aromaticity (HOMA) index,[44,45] the multicenter index (MCI),[46] the aromatic fluctuation index (FLU),[47] the anisotropy of the induced current density (ACID) plots,[48,49] and the nucleus-independent chemical shifts (NICS)-*XY* scans[50,51] were used to quantify the aromatic character of the different systems. The correlation between the aromaticity indexes has been challenged;[52] here we chose to report several indexes for completeness. All five indices of aromaticity were computed at the (U)B3LYP/6-311+G(d,p) level at the PBE0/6-311+G(d,p) geometries.

The HOMA is defined as:

$$HOMA = 1 - \frac{1}{n}\sum_{i=1}^{n} \alpha_{opt}\left(R_{opt} - R_i\right)^2 \quad (1)$$

where *n* is the number of bonds considered, α is an empirical constant (for C–C, C–N, C–O, C–S, and N–N bonds α = 257.7, 93.5, 157.4, 94.1, and 94.09, respectively),[53] R_{opt} is an optimal bond value (1.388, 1.334, 1.265, 1.667, and 1.309 Å for C–C, C–N, C–O, C–S, and N–N bonds, respectively) and R_i stands for a running bond length.

FLU was computed using delocalization indices, δ(A,B), with the expression:

$$FLU(\mathcal{A}) = \frac{1}{N}\sum_{i=1}^{N}\left[\left(\frac{V(A_i)}{V(A_{i-1})}\right)^{\alpha}\left(\frac{\delta(A_i,A_{i-1}) - \delta_{ref}(A_i,A_{i-1})}{\delta_{ref}(A_i,A_{i-1})}\right)\right]^2 \quad (2)$$

where $A_0 \equiv A_N$ and the string $\mathcal{A} = \{A_1, A_2, \ldots, A_N\}$ contains the ordered elements according to the connectivity of the N atoms in a ring or in a chosen circuit. V(A) is defined as:

$$V(A_i) = \sum_{A_j \neq A_i} \delta\left(A_i, A_j\right) \quad (3)$$

and α is a simple function to make sure that the first term is always greater than or equal to 1. The delocalization indices of Eq. 1 were calculated using the overlaps between occupied molecular orbitals in the atomic basins generated by AIMAll program.[54] The $\delta_{ref}(C,C)$, $\delta_{ref}(C,\mathrm{N})$, $\delta_{ref}(C,\mathrm{O})$ and $\delta_{ref}(C,S)$ reference values of 1.389 e, 1.113 e, 0.971 e and 1.270 e used for C–C, C–N, C–O and C–S bonds, respectively, in FLU calculations corresponds to the $\delta(C,C)$ of benzene, $\delta(C,N)$ of pyridine, $\delta(C,O)$ of furan and $\delta(C,S)$ of thiophene computed at the B3LYP/6-311+G(d,p) level of theory. FLU is close to 0 in aromatic species, and differs from it in non-aromatic ones.

The MCI is an electronic index obtained from I_{ring} values as follows:

$$MCI(\mathcal{A}) = \frac{1}{2N}\sum_{P(\mathcal{A})} I_{ring}(\mathcal{A}) \quad (4)$$

where $P(\mathcal{A})$ stands for a permutation operator which interchanges the atomic labels A_1, A_2 ... A_N to generate up to the *N*! permutations of the elements in the string $\mathcal{A}$, and the I_{ring} index is defined as:

$$I_{ring}(\mathcal{A}) = \sum_{i_1,i_2,\ldots i_N} n_{i_1} \ldots n_{i_N} S_{i_1 i_2}(A_1) S_{i_2 i_3}(A_2) \ldots S_{i_N i_1}(A_N) \quad (5)$$

where $S_{ij}(A)$ is the overlap of natural orbitals *i* and *j* in the atom *A* defined in the framework of the QTAIM,[55] and n_i are their occupancies. FLU and MCI indices were obtained with the ESI program.[56] NICS-*XY* scans were performed using the Aroma package.[51] These were computed at 1.7Å above the plane of the molecules using the σ-only model to retrieve the π-contributions.

Results and discussion

The symmetric dibenzannelated compounds **1a** – **1c** with central seven-membered 8π-electron cycles are analyzed first. These compounds have only one heteroatom, and two of them have earlier been studied experimentally by Shukla and Wan.[31] We then consider compounds **1d** – **1g** that have either two or three heteroatoms in the central 8π-electron cycle. These compounds allow us to probe the limitations of the excited state aromaticity concept because gradually more nπ* states can now compete with the lowest and potentially Baird-aromatic ππ* states for being the T_1 and S_1 states. At the end we briefly analyze the dibenzannelated six-membered heterocycles with eight π-electron cores (**2a** – **2d**) which all have two heteroatoms in the central ring. In three of these, nπ* states can be the T_1 and S_1 states.

Compounds 1a – 1c: In their S_0 states, these compounds are markedly puckered with benzene rings that display clear signatures of aromaticity. The bond lengths in these rings are 1.388 – 1.407 Å (**1a**), 1.379 – 1.401 Å (**1b**) and 1.386 – 1.405 Å (**1c**), respectively, corresponding to strong aromatic character as the HOMA values approach 1.0 (Figure 5). For further details on the aromaticity of **1a** – **1c** in their S_0 states see the Supporting Information.

In contrast to the S_0 states, in their T_1 and S_1 states compounds **1a** and **1b** are planar and C_{2v} symmetric and **1c** is nearly planar (C_s symmetric with a minute puckering at the S atom). Moreover, the T_1 state geometry of each individual compound strongly resembles the S_1 state geometry, indicating that the two states, apart from the difference in multiplicity, are of the same character. Also, when regarding the CC bond lengths of the three compounds in the T_1 and S_1 states one can only see minute variations between the three compounds (Figure 6). For the S_1 state, CC bond lengths in the perimeters are found in the ranges 1.369 – 1.425 Å (**1a**), 1.368 – 1.427 Å (**1b**), and 1.367 – 1.430 Å (**1c**), respectively, and the same applies to the T_1 state. The strong resemblance in geometries suggest that the S_1 and T_1 states in **1b** and **1c** are of ππ* character, just like in in **1a** where there is no competing nπ* excited state.

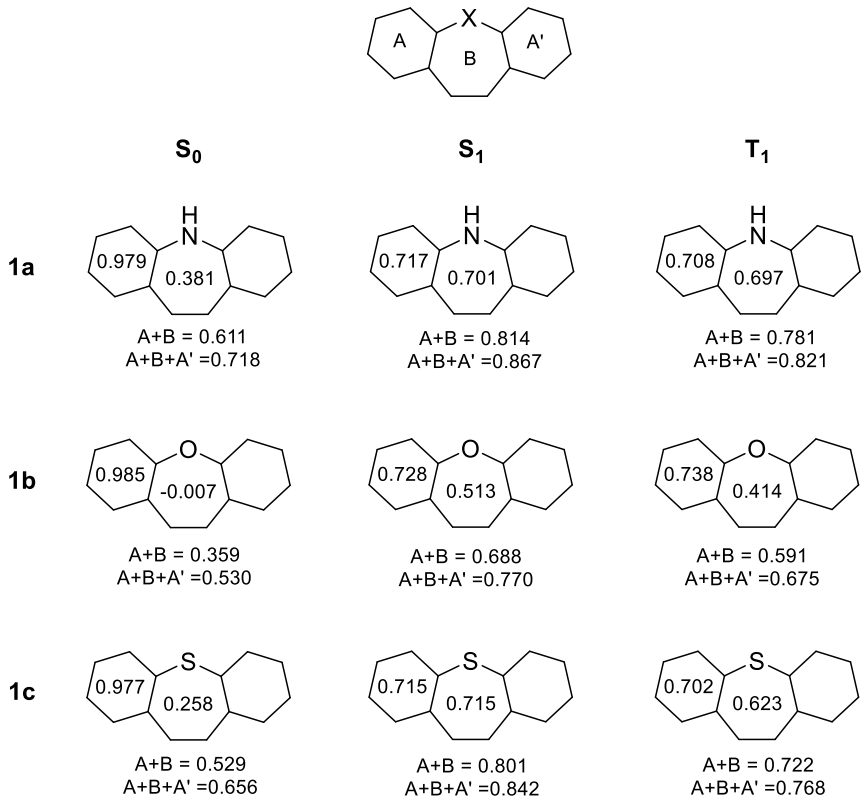

Figure 5: HOMA values for **1a**, **1b** and **1c** in the S_0, S_1 and, T_1 states at PBE0/6-311+G(d,p) level. TD-PBE0 was used for the S_1 states and UPBE0 for the T_1 states.

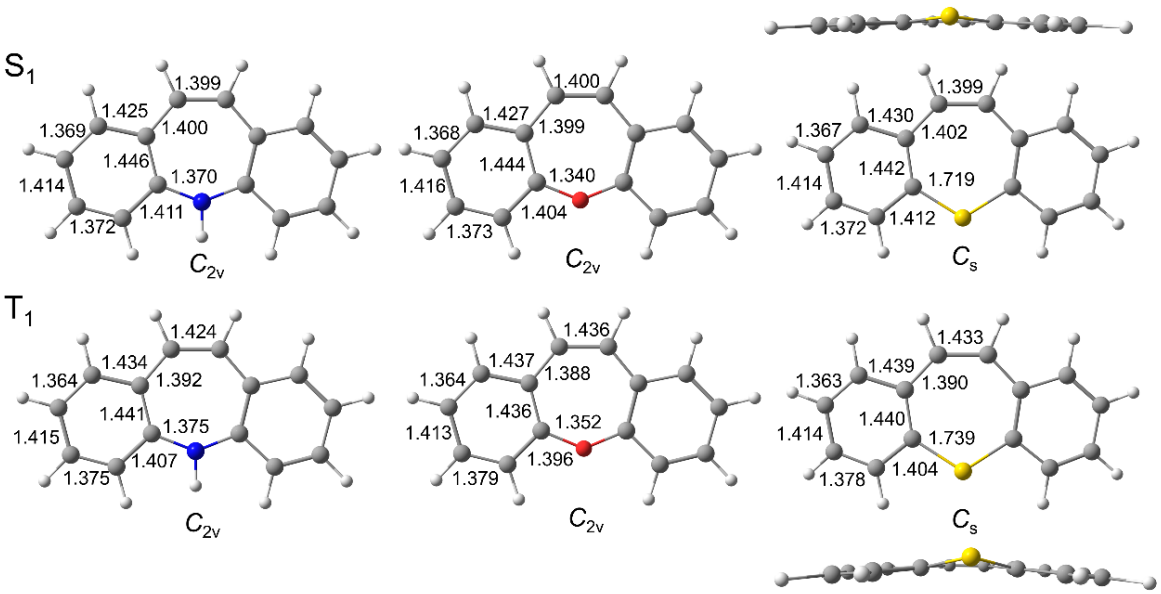

Figure 6: Geometries of **1a** – **1c** in their T_1 and S_1 states at PBE0/6-311+G(d,p) level. TD-PBE0 was used for the S_1 states and UPBE0 for the T_1 states. Bond distances are given in Å.

Indeed, an analysis of the orbitals and the electron configurations reveal the similarity between the S_1 and T_1 states; they are all of singly-excited (HOMO to LUMO) $\pi\pi^*$ character (Figure 7 for orbitals of **1b**) at both TD-PBE0 and CASSCF/CASPT2 levels (see the Supporting Information). Furthermore, a plot of the energy changes of the S_0, S_1 and S_2 states, starting at the vertically excited and going to the relaxed S_1 state structures, reveals that there is no state crossing along the relaxation pathways for the compounds (Figures 8). The lowest state reached upon vertical excitation is the same state as the relaxed S_1 state. For **1b**, the calculated vertical absorption (λ_{abs} = 304 nm) and emission (λ_{em} = 530 nm) wavelengths are in reasonable agreement with UV-Vis experimental data (λ_{abs} = 280 nm and λ_{em} = 478 nm in cyclohexane). The differences between the experimental and calculated transitions correspond to 0.35 eV for the absorption and 0.25 eV for the emission.

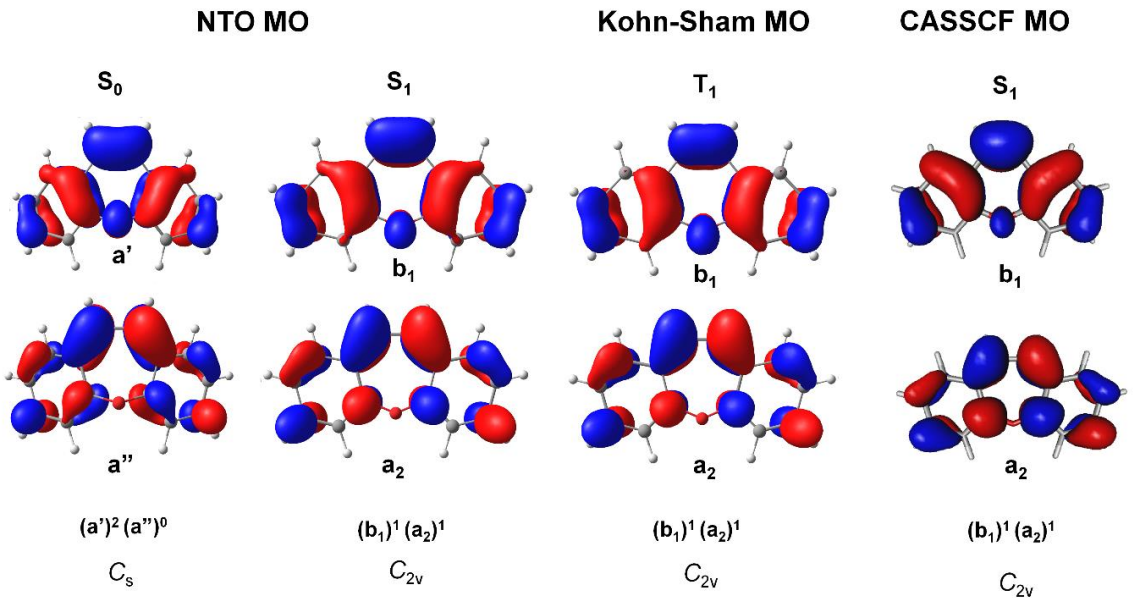

Figure 7: Plots of molecular orbitals and their respective symmetries involved in the electronic transitions in the S_0, S_1, and T_1 geometries of **1b** and respective electronic configurations. The natural transition orbitals (NTO) and Kohn-Sham MOs were computed at ωB97XD/6-311+G(d,p) level and natural orbitals were computed using the CASSCF wave function.

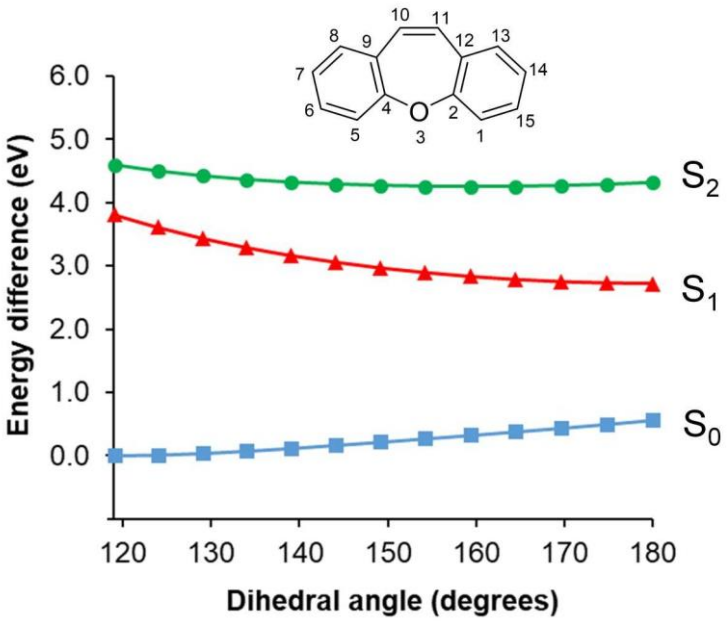

Figure 8: Changes in the energies of the S_0, S_1 and S_2 states of **1b** along the relaxation pathway from the vertically excited structure to the relaxed S_1 state structure, here defined as the C5-C4-O3-C2 dihedral angle.

Now, are the T_1 and S_1 states aromatic? When going from the S_0 state to the first excited states the HOMA values (Figure 6) increase significantly for the central ring (B ring) while they decrease for the outer benzene rings. This indicates a gain in aromaticity in the central rings. When comparing the three compounds, the HOMA values of the B rings are distinctly larger in **1a** and **1c** than in **1b** in both S_1 and T_1, and the same pattern applies to the perimeters (A+B+A') as well as the 12π-electron two-ring circuits (A+B). According to HOMA **1a** and **1c** are thus the more excited state aromatic compounds. Interestingly, the HOMA values for the various 4*n*π-electron circuits in the T_1 state are always slightly lower than the values for the corresponding circuits in the S_1 state. Among the various circuits, the perimeters always have the highest HOMA values among the investigated possible 4*n*π-electron circuits in both the T_1 and S_1 states, suggesting that the global aromaticity is the most important.

The electron density based indices FLU and MCI reveal the degree of π-electron delocalization in the various rings of **1a** – **1c**. For the three compounds in their T_1 states the small FLU values along the perimeters indicate that the delocalization is more efficient along the 16π-electron circuits than in the central 8π-electron rings (Table 1), in line with observations from HOMA. For **1a** and **1b** the circuits containing twelve π-electrons (A+B and B+A') have intermediate values when compared to the perimeters and the B rings, whereas for **1c** all circuits have similar FLU values as the perimeter. Regarding the MCI values, we first note that the S_1 and T_1 states for each of the three molecules have similar MCI values when calculated with TD-DFT and DFT (Table 2), respectively. On the other hand, the MCI values from CASSCF calculations are too small, revealing the importance of dynamic electron correlation, as was previously observed by Solà and coworkers.[8,57] When comparing the three compounds, the MCI values for the T_1 and S_1 states are larger for the azepine ring in **1a** than for the oxepine ring in **1b**, indicating that the local aromaticity of the former is larger. The MCI values for the thiepine ring in **1c** in T_1 and S_1 are intermediate. Interestingly, this is the same

order in degree of aromaticity as found in the S_0 states of pyrrole, furan, and thiophene, and should reflect the relative energy and size of the 2p or 3p lone-pair orbital of the X atom leading to differences in π-orbital overlap with adjacent C atoms. It can also be noted that the aromatic character of the benzene rings in **1a** – **1c** when the three compounds are excited decrease in the aromatic characters according to MCI. As the MCI values in the T_1 and S_1 states for the benzene rings are similar this further reveals the resemblance between the two states.

Table 1. FLU index values computed for the planar and near-planar molecules in their T_1 states. A and A' represent the two equivalent benzenoid rings and B the central ring.[a]

	A (A')	**B**	**A+B**	**A+B+A'**
1a	0.015	0.018	0.013	0.010
1b	0.015	0.019	0.013	0.011
1c	0.013	0.011	0.008	0.009

[a] Compounds **1a** and **1b** are C_{2v} and **1c** C_s symmetric.

Table 2. MCI indexes (in electrons) computed for the planar and near-planar molecules for the ground (S_0), first excited singlet (S_1), and first excited triplet (T_1) state. Letters A and A' indicate the two benzenoid rings and B indicates the central ring. The S_0 and T_1 states were calculated with DFT and the S_1 state with TD-DFT and CASSCF (in italics).

	S_0		**S_1**		**T_1**	
	A (A')	**B**	**A (A')**	**B**	**A (A')**	**B**
1a	0.0545	0.0013	0.0249	0.0024	0.0259	0.0062
			0.0152	*0.0019*		
1b	0.0569	0.001	0.0251	0.0016	0.0276	0.0034
			0.0121	*0.0006*		

1c	0.0583	0.001	0.0271	0.0022	0.0276	0.0051
			0.0147	*0.0020*		

The magnetic aromaticity indicators calculated for the T_1 state in each of the three compounds further corroborate their excited state aromatic character. NICS-*XY* plots are shown in Figure 9 for **1a - 1c**. The NICS-*XY* values in the center of the B rings are -22.7, -15.2 and -15.4 ppm for **1a**, **1b**, and **1c,** respectively, suggesting that the nitrogen-containing heterocycle is more aromatic than the others, in agreement with the MCI, FLU, and HOMA results. Yet, thiepine **1c** has a slightly less negative value than oxepine **1b**. By also calculating the NICS-*XY* scan (Figure S13) for the C_{2v} symmetric structure of **1c** (a structure with one imaginary frequency) we can attribute the slightly lowered excited state aromaticity of **1c** to the minute puckering around the S atom. The NICS plots also reveal a global aromaticity for these three molecules, similarly to dibenzocyclooctatetraene reported by Ayub *et al.*,[33] although the central 8π-electron ring makes a substantial contribution to the triplet state aromatic character.

ACID plots using the total contributions (σ and π) indicate the predominance of global aromaticity in **1a** - **1c** (Figure 10A). Yet, the opposite pattern is revealed in the π-only ACID because the global currents are weakened and the local ones in the B rings are enhanced (Figure 10b). Thus, by removing the σ-contribution, which is not of relevance for the aromaticity in these compounds, one can clearly see the diatropic ring in the central 8π-electron system. The π-ACID model indicates that the global aromaticity is larger for **1b** and **1c**, in agreement with what is found based on the HOMA values for the perimeter.

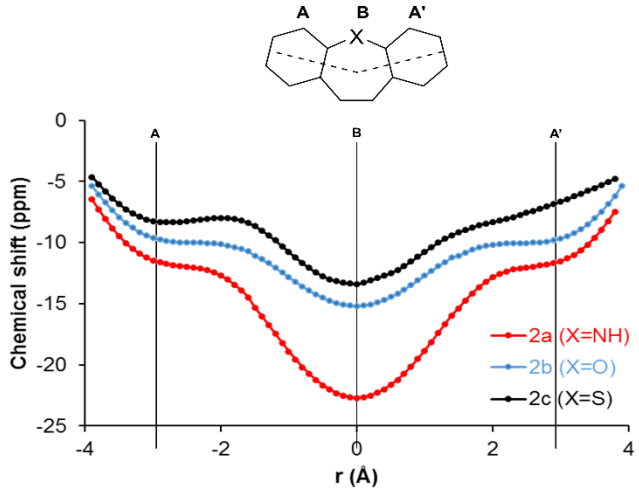

Figure 9: NICS-*XY* scans of **1a** – **1c** in their T_1 states calculated at GIAO-UB3LYP/6-311+G(d,p)//UPBE0/6-311+G(d,p) level.

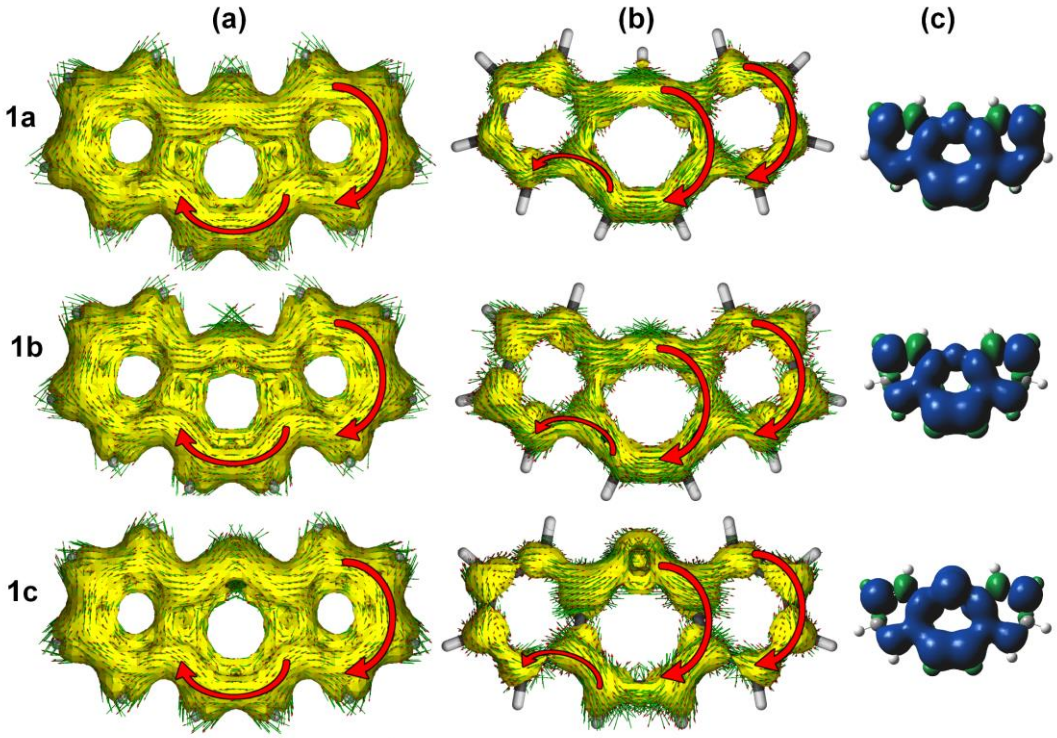

Figure 10: ACID plots in the T_1 state for **1a**, **1b**, and **1c** at the UB3LYP/6-311+G(d,p)//UPBE0/6-311+G(d,p) level: (a) σ + π contribution; (b) π contribution, (c) T_1 state isospin density map calculated at UB3LYP/6-311+G(d,p)//UPBE0/6-311+G(d,p) level. Full-scale ACID plots are found in the Supporting Information.

To conclude, **1a** – **1c** are all aromatic in their T_1 and S_1 states. Whether the dominating aromatic cycle is the central 8π-electron heterocycle or the perimeter varies to some extent between the compounds and between aromaticity index used. Plots of spin density, NICS-*XY* scans, HOMA and FLU indices favor the presence of a global 16π-electron circuit, in a similar way that biphenylene shows a global 12π-electron circuit in its T_1 state.[33] Yet, the 8π-electron circuit becomes dominating when regarding the π-only contribution to the ACID, in line with the interpretation given by Shukla and Wan.[31] The three compounds can obviously be labelled as aromatic chameleon compounds, i.e., they can adapt their electron distribution to as to comply with the different aromaticity rules in different electronic states.

Compounds 1d – 1g: Now what is the case of the dibenzannelated compounds with several heteroatoms in the central 8π-electron 7MR? Here, the non-annelated C=C double bond was changed to an N=C bond (**1d** – **1f**) or an N=N bond (**1g**), providing more σ-type lone-pairs from which excitations may occur. The first three in the set are also unsymmetric in the sense that the two benzene rings are non-equivalent.

The geometries of these four compounds in their T_1 and S_1 states reflect the differences between compounds with ππ* versus those with nπ* states as the lowest excited states. Compounds **1d** and **1e** are planar in both T_1 and S_1 states while **1f** is slightly puckered in S_1 (like **1c**, both with X = S) and more distinctly so in T_1 (for optimized geometries see Figure S2) However, **1g** is even more strongly puckered in both excited states.

Now, with regard to the aromaticity in the excited states of **1d** – **1f** we can note the same pattern as for the **1a** – **1c** compounds. Starting with HOMA, **1d** is the most aromatic in both the T_1 and S_1 states. In general, the HOMA values for all circuits of **1d**, **1e**, and **1f**, respectively, closely resemble the corresponding HOMA values of **1a**, **1b** and **1c**, respectively. This applies to both the T_1 and S_1 states, and also **1d** – **1f** are slightly more aromatic in their S_1

states than in their T_1 states when based on HOMA. When considering the electron density based indices (FLU and MCI) we can again see a strong resemblance within each of the pairs **1a**/**1d**, **1b**/**1e**, and **1c**/**1f**. Finally, with regard to NICS-*XY* it was only run for **1d** and **1f**, yet these compounds in their T_1 states again show a close resemblance with **1a** and **1b** in the T_1 states, and this is also in line with the ACID plots.

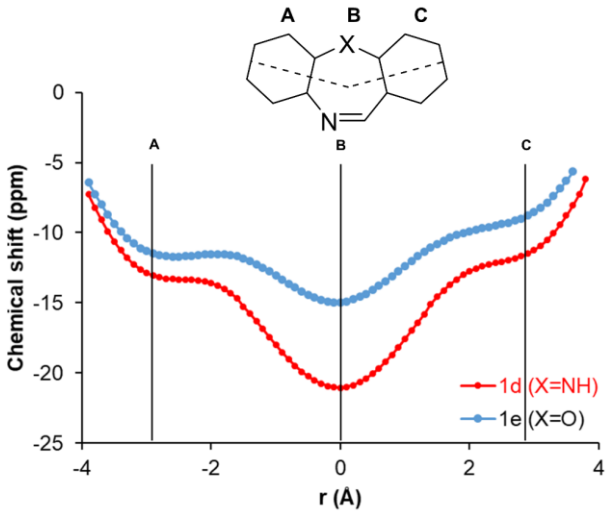

Figure 11: NICS-*XY* scans of **1d** – **1e** in their T_1 states (σ only model) calculated at GIAO-UB3LYP/6-311+G(d,p)//UPBE0/6-311+G(d,p) level level.

Table 3. MCI indexes (in electrons) for **1d** – **1g** in the S_0, S_1, and T_1 states computed at (TD)-B3LYP/6-311+G(d,p)//PBE0/6-311+G(d,p) levels.[a]

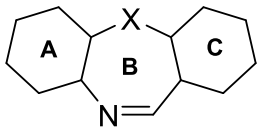

	S_0			S_1			T_1		
	A	**B**	**C**	**A**	**B**	**C**	**A**	**B**	**C**
1d	0.0541	0.0011	0.0541	0.0247	0.0022	0.0264	0.0230	0.0061	0.0278
1e	0.0559	0.0009	0.0559	0.0241	0.0016	0.0263	0.0228	0.0037	0.0296
				0.0118	*0.0007*	*0.0130*			
1f	0.0566	0.0008	0.0598	0.0271	0.0021	0.0288	0.0244	0.0040	0.0332
1g	0.0535	0.0011	0.0535				0.0449	0.0007	0.449

[a] In italics: calculated using CASSCF wavefunction.

Compound **1g** with three heteroatoms in the central ring has a highly puckered structure in the T_1 state. Still, **1g** in this state has high HOMA values for the central ring (0.798, see Figure S12) as well as for the perimeter (0.917). One could thus argue based on HOMA that **1g** is Baird-aromatic, however, all other aromaticity indices tell the opposite. The ACID plot reveals strong diatropic ring currents localized to the two outer benzene rings corresponding to closed-shell Hückel aromaticity (for spin density see the Supporting Information). Additionally, the FLU and MCI indices unambiguously tell that the benzene rings are the aromatic cycles, particularly as the MCI values of these rings in the T_1 state resemble those of the S_0 state.

To sum up, the introduction of one additional N atom as compared to the azepine has no extensive effect on the excited state aromaticity, yet, a N=N double bonded segment in the central 8π-electron cycle leads to nπ* states as the lowest excited states (see Supporting Information).

Compounds 2a – 2d: Three of these molecules are puckered in their S_0 states while the forth one (dibenzodioxin, **2d**) has a planar D_{2h} symmetric structure. Yet, the degree of puckering in **2a** – **2c** is smaller than for **1a** – **1g**. Now, to what extent do they planarize in the lowest excited states? Or does the planar one (**2d**) distort to nonplanarity in the excited states? Due to significant multiconfigurational character of the singlet excited states of **2a** – **2d** we only consider the T_1 states here and make comparisons with the T_1 states of **1a** – **1g**. Similar as for **1a**, compound **2a** has no in-plane lone-pair electrons and will therefore only have ππ* states among its manifold of lowest excited states.

The structures of **2a** and **2b** are both planar with **2a** having D_{2h} symmetry whereas the symmetry of **2b**, on the other hand, varies with functional used. With ωB97XD it is C_{2v} symmetric, but with PBE0 it is only C_s symmetric as one of the O atoms is shifted off the C_2

rotational axis towards one of the two adjacent C atoms. Compound **2c** is again C_s symmetric, yet, instead has a slight puckering at the S atom so that the two benzene rings are equivalent.

The NICS-*XY* scans of **2a** – **2c** in the T_1 states shows strong resemblance between the three compounds as the negative NICS values, corresponding to diatropic (aromatic) ring-currents, are markedly localized to the B ring (Figure 12). The benzene rings in **2b** and **2c** even have NICS values that correspond to weak antiaromatic character. This picture is reinforced further through the π-only contributions of the ACID plot because a strong diatropic ring-current is visible in the ring B while in rings A and A' one can instead observe local paratropic ring-currents that merge with the diatropic ring-current of ring B in the two CC bonds between the rings (see Figure S11 for the π-only ACID of **2a** in the T_1 state). This picture is starkly different from that of compounds **1a** – **1g**. When considering the MCI values in the S_1 and T_1 states we observe that the values for the central ring are larger while the values for the two outer benzene rings are smaller than for the previous molecules in their T_1 states.

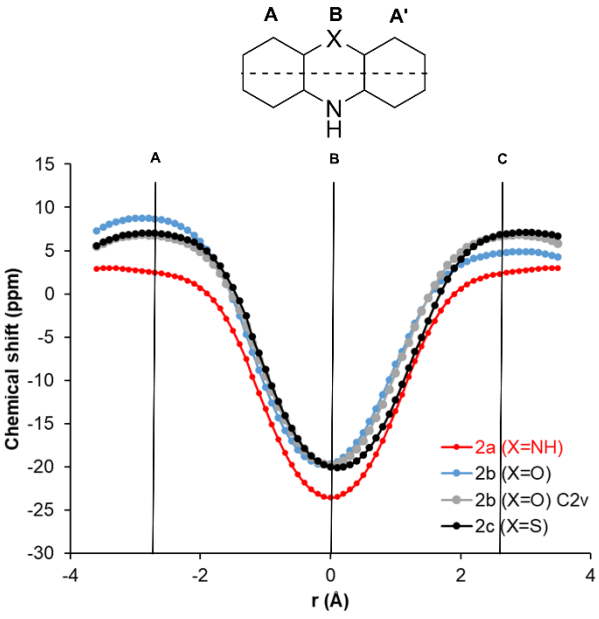

Figure 12: NICS-*XY* scans of **2a** – **2c** in their T_1 states (σ only model) calculated at GIAO-UB3LYP/6-311+G(d,p)//UPBE0/6-311+G(d,p) level level.

Finally, with regard to **2d** this molecule is both non-planar and unsymmetric in its T_1 state according to PBE0/6-311+G(d,p) calculations, and it has a particularly strong distortion around one of the oxygen atoms. Similarly highly unsymmetric T_1 state structures are found also with the B3LYP and ωB97XD methods. Thus, the T_1 state according to UDFT is clearly of nπ* character. On the other hand, earlier CASSCF calculations have described it as a planar and D_{2h} symmetric molecule.[58] For the much smaller dioxin molecule we find that the structure (planar vs. nonplanar) varies extensively with method with methods including dynamic electron correlation (CASPT2 and the DFT methods) leading to a nonsymmetric structure. Whether dibenzodioxin is planar in its lowest excited states, or not, seems to require a dedicated effort focused on this molecule.

Table 4. MCI indexes (in electrons) computed at (TD)-B3LYP/6-311+G(d,p)//PBE0/6-311+G(d,p) level for molecules **2a** – **2d** for the ground (S_0), first excited singlet (S_1), and first excited triplet (T_1) state.

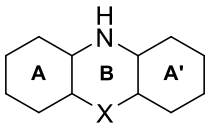

	S_0		**S_1**		**T_1**		
	A / A'	**B**	**A / A'**	**B**	**A**	**B**	**A'**
2a	0.0523	0.0022	0.0205	0.0014	0.0193	0.0071	0.0193
2b	0.0551	0.0019	0.0212	0.0012	0.0177 [a] 0.0196 [b]	0.0054 [a] 0.0054 [b]	0.0215 [a] 0.0196 [b]
2c	0.0562	0.0019	0.0227 *0.0129*	0.0016 *0.0011*	0.0210	0.0082	0.0210
2d	0.0576	0.0019	0.0218	*0.0012*	0.0051	0.0019	0.0480

[a] The T_1 state structure of **2b** is not symmetric. [b] The T_1 state structure of **2d** is not planar.

Conclusions

Many dibenzannelated 8π-electron heterocyclic molecules are influenced by aromaticity both in their S_0 states and in their lowest excited states (S_1 and T_1). In the S_0 states, the two benzene rings are strongly Hückel-aromatic while in the S_1 and T_1 states the central 8π-electron cycle and/or the 16π-electron perimeter can be Baird-aromatic. The requirement for the latter is that the S_1 and T_1 state have ππ* instead of nπ* character, and according to quantum chemical calculations this is the situation when the central cycle has either one or two heteroatoms. The compounds that are aromatic in their S_1 and T_1 states also adopt planar or nearly planar excited state structures.

Yet, molecules with S_1 and T_1 states having nπ* character, as found in the dibenzannelated compound with N=N bonds and in dibenzodioxin, are strongly puckered in these states and they are nonaromatic. On the other hand, compounds with isolated N atoms in the heterocycles, either as -NR- or as -N=CH-, provide for the most strongly excited state aromatic compounds, hence resembling the situation in the S_0 state with pyrrole being more aromatic than furan and thiophene. A further difference exists between compounds with central seven-membered versus those with six-membered 8π-electron heterocycles as the former tend to have the 16π-electron perimeter as the strongest aromatic circuit while the latter ones have the central ring as the most aromatic circuit.

On the experimental side, the planarization that is observed in the excited state results in large Stokes' shifted emissions as observed by Shukla and Wan.[31] Such large Stokes' shift should indeed be general for many dibenzannelated 8π-electron heterocycles.

Acknowledgements

The Foundation Olle Engkvist Byggmästare is greatly acknowledged for a postdoctoral fellowship to J.T. (grant 184-390) and the Wenner-Gren Foundations is greatly acknowledged

for a postdoctoral fellowship to O.E.B. (grant UPD2017-0243). The authors are grateful to Dr. Ferran Feixas for helpful discussions on the use of the ESI-3D program. H.O. is grateful to the Vinnova agency for an academia-industry exchange grant (2016-04572). The computations were performed on resources provided by the Swedish National Infrastructure for Computing (SNIC) at NSC and UPPMAX. M.S. acknowledges the financial support from the Spanish MINECO (project CTQ2017-85341-P), the Catalan DIUE (2017SGR39, XRQTC, and ICREA Academia 2014 Award to M.S.), and the FEDER fund (UNGI10-4E-801).

References

[1] R. Gleiter, G. Haberhauer, Aromaticity and Other Conjugation Effects, Wiley-VCH, 2012.

[2] E. Hückel, *Zeitschrift f. Physik*, **1931**, *70*, 204-286.

[3] N. C. Baird, *J. Am. Chem. Soc.* **1972**, *94*, 4941-4948.

[4] H. Ottosson, *Nat. Chem.* **2012**, *4*, 969-971.

[5] M. Rosenberg, C. Dahlstrand, K. Kilså, H. Ottosson, *Chem. Rev*., **2014**, *114*, 5379-5425.

[6] R. Papadakis, H. Ottosson, *Chem. Soc. Rev*. **2015**, *44*, 6472-6493.

[7] (a) P. B. Karadakov, *J. Phys. Chem. A* **2008**, *112*, 7303-7309. (b) P. B. Karadakov, *J. Phys. Chem. A* **2008**, *112*, 12707-12713. (c) P. B. Karadakov, P. Hearnshaw, K. E. Horner *J. Org. Chem.* **2016**, *81*, 11346-11352, (d) P. B. Karadakov, M. A.H. Al-Yassiri, D. L. Cooper *Chem. Eur. J.* **2018**, *24*, 16791-16803.

[8] F. Feixas, J. Vandenbussche, P. Bultinck, E. Matito, M. Solà, *Phys. Chem. Chem. Phys.*, **2011**, *13*, 20690-20703.

[9] M. Hada, S. Saito, S. Tanaka, R. Sato, M. Yoshimura, K. Mouri, K. Matsuo, S. Yamaguchi, M. Hara, Y. Hayashi, F. Röhricht, R. Herges, Y. Shigeta, K. Onda, R. J. D. Miller, *J. Am. Chem. Soc.* **2017**, 139, 15792-15800.

[10] (a) T. Yamakado, S. Takahashi, K. Watanabe, Y. Matsumoto, A. Osuka, S. Saito, *Angew. Chemie Inter. Ed.* **2018**, *57*, 5438-5443. (b) M. Hada, S. Saito, S. i. Tanaka, R. Sato, M. Yoshimura, K. Mouri, K. Matsuo, S. Yamaguchi, M. Hara, Y. Hayashi, F. Röhricht, R. Herges, Y. Shigeta, K. Onda, R. J. D. Miller, *J. Am. Chem. Soc.* **2017**, *139*, 15792-15800; (c) R. Kotani, H. Sotome, H. Okajima, S. Yokoyama, Y. Nakaike, A. Kashiwagi, C. Mori, Y. Nakada, S. Yamaguchi, A. Osuka, A. Sakamoto, H. Miyasaka, S. Saito, *J. Mat. Chem. C* **2017**, *5*, 5248-5256.

[11] S. Chen, N. Ullah, R. Zhang, *J. Phys. Chem. Lett.* **2018**, *17*, 4857-4864.

[12] J. Wu, I. Fernandez, Y. Mo, P. v. R. Schleyer, *J. Chem. Theory Comput.* **2012**, *8*, 1280-1287.

[13] A. Toyota, S. Koseki, H. Umeda, M. Suzuki, K. Fujimoto, *J. Phys. Chem. A* **2003**, *107*, 2749-2756.

[14] C. Dardonville, M. L. Jimeno, I. Alkorta, J. Elguero, *Org. Biomol. Chem.* **2004**, *2*, 1587-1591.

[15] C. C. Pye, J. D. Xidos, R. A. Poirier, D. J. Burnell, *J. Phys. Chem. A* **1997**, *101*, 3371-3376.

[16] H. Jansen, J. C. Slootweg, K. Lammertsma, *Beilstein J. Org. Chem.* **2011**, *7*, 1713-1721.

[17] H. H. Eckhardt, D. Hege, W. Massa, H. Perst, R. Schmidt, *Angew. Chem. Int. Ed*. **1981**, *20*, 699-701.

[18] M. J. McManus, G. A. Berchtold, D. R. Boyd, D. A. Kennedy, J. Malone, *J. Org. Chem.* **1986**, *51*, 2784-2787.

[19] K. Yamamoto, S. Yamazaki, Y. Kohashi, I. Murata, Y. Kai, N. Kanehisa, K. Miki, N. Kasai, *Tetrahedron Lett.* **1982**, 23, 3195-3198.

[20] B. A. Hess, L. J. Schaad, C. W. Holyoke, *Tetrahedron* **1972**, *28*, 3657-3667.

[21] M. J. S. Dewar, N. Trinajstić, *Tetrahedron* **1970**, *26*, 4269-4276.

[22] C. Foroutan-Nejad, S. Shahbazian, P. Rashidi-Ranjbar, *Phys. Chem. Chem. Phys.* **2010**, *12*, 12630-12637.

[23] C. Glidewell, D. Lloyd, *Tetrahedron* **1984**, *40*, 4455-4472.

[24] O. El Bakouri, J. Poater, F. Feixas, M. Solà, *Theor. Chem. Acc.* **2016**, *135*, 205.

[25] (a) C. Bodea, I. Silberg, in *Advances in Heterocyclic Chemistry, Vol. 9* (Eds.: A. R. Katritzky, A. J. Boulton), Academic Press, **1968**, pp. 321-460. (b) M. Malińska, J. Nowacki, A. Kapturkiewicz, K. Woźniak, *RSC Advances* **2012**, *2*, 4318-4328.

[26] V. Gogonea, P. v. R. Schleyer, P. Schreiner, *Angew. Chem., Int. Ed.* **1998**, *37*, 1945-1948.

[27] M. Garavelli, F. Bernardi, A.Cembran, O. Castaño, L. M. Frutos, M. Merchán, M. Olivucci, *J. Am. Chem. Soc.* **2002**, *124*, 13770-13789.

[28] S. Villaume, H. A. Fogarty, H. Ottosson, *ChemPhysChem* **2008**, *9*, 257-264.

[29] (a) P. J. Forward, A. A. Gorman, I. Hamblett, *J. Chem. Soc., Chem. Commun*. **1993**, 250-251. (b) T. N. Das, I. Priyadarsini, *J. Chem. Soc. Faraday Trans.* **1994**, *90*, 963-968.

[30] M. Ueda, K. Jorner, Y. M. Sung, T. Mori, Q. Xiao, D. Kim, H. Ottosson, T. Aida, Y. Itoh, *Nat. Comm.* **2017**, *8*, 346.

[31] D. Shukla, P. Wan, *J. Am. Chem. Soc.* **1993**, *115*, 2990-2991.

[32] H. Möllerstedt, M. C. Piqueras, R. Crespo, H. Ottosson, *J. Am. Chem. Soc.*, 2004, **126**, 13938-13939.

[33] R. Ayub, O. E. Bakouri, K. Jorner, M. Solà, H. Ottosson, *J. Org. Chem.* **2017**, *82*, 6327-6340.

[34] J. Perdew, M. Ernzerhof, K. Burke, *J. Chem. Phys*., **1996**, *105*, 9982.

[35] R. Krishnan, J. S. Binkley, R. Seeger J. A. Pople, *J. Chem. Phys*., **1980**, *72*, 650-654.

[36] S. Grimme, J. Antony, S. Ehrlich, H. Krieg, *J. Chem. Phys*., **2010**, *132*, 154104.

[37] D. Bousquet, R. Fukuda, D. Jacquemin, I. Ciofini, C. Adamo, M. Ehara, *J. Chem. Theory Comput.*, **2014**, *10*, 3969-3979.

[38] E. Brémond, M. Savarese, C. Adamo, D. Jacquemin, *J. Chem. Theory Comput.*, **2018**, *14*, 3715-3727.

[39] D. Bousquet, R. Fukuda, P. Maitarad, D. Jacquemin, I. Ciofini, C. Adamo, M. Ehara, *J. Chem. Theory Comput.*, **2013,** *9*, 2368-2379.

[40] D. Shukla, P. Wan, *J. Am. Chem. Soc.* **1993**, *115*, 2990-2991.

[41] E. Matito, M. Solà, P. Salvador, M. Duran, *Faraday Discuss.* **2007**, *135*, 325-345.

[42] Gaussian 16, Revision B.01, M. J. Frisch, G. W. Trucks, H. B. Schlegel, G. E. Scuseria, M. A. Robb, J. R. Cheeseman, G. Scalmani, V. Barone, G. A. Petersson, H. Nakatsuji, X. Li, M. Caricato, A. V. Marenich, J. Bloino, B. G. Janesko, R. Gomperts, B. Mennucci, H. P. Hratchian, J. V. Ortiz, A. F. Izmaylov, J. L. Sonnenberg, D. Williams-Young, F. Ding, F. Lipparini, F. Egidi, J. Goings, B. Peng, A. Petrone, T. Henderson, D. Ranasinghe, V. G. Zakrzewski, J. Gao, N. Rega, G. Zheng, W. Liang, M. Hada, M. Ehara, K. Toyota, R. Fukuda, J. Hasegawa, M. Ishida, T. Nakajima, Y. Honda, O. Kitao, H. Nakai, T. Vreven, K. Throssell, J. A. Montgomery, Jr., J. E. Peralta, F. Ogliaro, M. J. Bearpark, J. J. Heyd, E. N. Brothers, K. N. Kudin, V. N. Staroverov, T. A. Keith, R. Kobayashi, J. Normand, K. Raghavachari, A. P. Rendell, J. C. Burant, S. S. Iyengar, J. Tomasi, M. Cossi, J. M. Millam, M. Klene, C. Adamo, R. Cammi, J. W. Ochterski, R.

L. Martin, K. Morokuma, O. Farkas, J. B. Foresman, D. J. Fox, Gaussian, Inc., Wallingford CT, **2016**.

[43] F. Aquilante, J. Autschbach, R. K. Carlson, L. F. Chibotaru, M. G. Delcey, L. De Vico, I.. Fdez. Galván, N. Ferré, L. M. Frutos, L. Gagliardi, M. Garavelli, A. Giussani, C. E. Hoyer, G. Li Manni, H. Lischka, D. Ma, P. Å. Malmqvist, T. Müller, A. Nenov, M. Olivucci, T. B. Pedersen, D. Peng, F. Plasser, B. Pritchard, M. Reiher, I. Rivalta, I. Schapiro, J. Segarra-Martí, M. Stenrup, D. G. Truhlar, L. Ungur, A. Valentini, S. Vancoillie, V. Veryazov, V. P. Vysotskiy, O. Weingart, F. Zapata, R. Lindh, *J. Comput. Chem.*, **2016**, *37*, 506-541.

[44] J. Kruszewski and T. M. M. Krygowski, *Tetrahedron Lett.*, **1972**, *13*, 3839-3842.

[45] T. M. Krygowski, *J. Chem. Inf. Model.*, **1993**, *33*, 70-78.

[46] P. Bultinck, M. Rafat, R. Ponec, B. Van Gheluwe, R. Carbó-Dorca P. Popelier, *J. Phys. Chem. A*, **2006**, *110*, 7642-7648.

[47] E. Matito, M. Duran, M. Solà, *J. Chem. Phys.*, **2005**, *122*, 014109. Erratum, íbid, **2006**, *125*, 059901.

[48] R. Herges, D. Geuenich, *J. Phys. Chem. A*, **2001**, *105*, 3214-3220.

[49] D. Geuenich, K. Hess, F. Köhler, R. Herges, *Chem. Rev.*, **2005**, *105*, 3758-3772.

[50] (a) R. Gershoni-Poranne, A. Stanger, *Chem. - Eur. J.*, **2014**, *20*, 5673-5688. (b) Stanger, *J. Org. Chem.*, 2010, **75**, 2281-2288. (c) A. Stanger, *J. Org. Chem.*, **2006**, *71*, 883-893.

[51] A. Stanger. A. Rahalkar, Aroma, http://schulich.technion.ac.il/Amnon_Stanger.htm.

[52] L. Zhao, R. Grande-Aztatzi, C. Foroutan-Nejad, J. M. Ugalde, G. Frenking, *Chem. Select* **2017**, *2*, 863-870.

[53] T. M. Krygowski, M. K. Cyrański, *Chem. Rev.*, **2001,** *101*, 1385-1420.

[54] AIMAll (Version 17.11.14 B) TK Gristmill Software (aim.tkgristmill.com), Overland Park KS, USA, 2018.

[55] R. F. W. Bader, *Atoms in Molecules: A Quantum Theory*, Clarendon, Oxford, 1990.

[56] E. Matito, ESI-3D: Electron Sharing Indexes Program for 3D Molecular Space Partitioning, Institute of Computational Chemistry and Catalysis, Girona, Catalonia, Spain, 2006, http://iqc.udg.es/~eduard/ESI.

[57] J. Poater, M. Solà, M. Duran, X. Fradera, *Theor. Chem. Acc.* **2002**, *107*, 362-371.

[58] I. Ljubic, A. Sabljic, *J. Phys. Chem. A* **2005**, *109*, 8209-8217.

Table of Contents

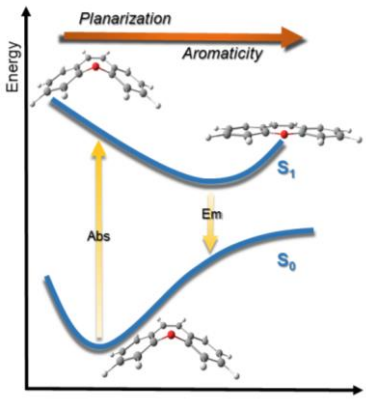

Striving for aromaticity: Dibenzannelated heterocyclic compounds with central 8π-electron rings are found in a range of different areas. The lowest excited states of such compounds can be aromatic according to Baird's 4*n* rule. Yet, when is that the case? We use quantum chemical calculations to evaluate if, and when changes in excited state geometries are driven by aromaticity.